Electron spin transport in graphene and carbon nanotubes

Tombros, Nikolaos

8

Electronic spin drift in graphene field effect transistors[1]

We studied the drift of electron spins under an applied DC electric field in single layer graphene spin valves in a field effect transport geometry at room temperature. In the metallic conduction regime ($n \simeq 3.5 \times 10^{16}$ m^{-2}), for DC fields of about ± 70 kV/m applied between the spin injector and spin detector, the spin valve signals are increased/decreased, depending on the direction of the DC field and the carrier type, by as much as $\pm 50\%$. Sign reversal of the drift effect is observed when switching from hole to electron conduction. In the vicinity of the Dirac neutrality point the drift effect is strongly suppressed. The experiments are in quantitative agreement with a drift-diffusion model of spin transport.

[1] C. Jozsa, M. Popinciuc, N. Tombros, H. T. Jonkman, B. J. van Wees, submitted to PRL

8.1 Introduction

Graphene, a two-dimensional hexagonal carbon lattice, was isolated from graphite and became available for electric transport type measurements in 2004 [1, 2]. Graphene is unique in its nature by allowing the experimentalist to shift the Fermi level trough the zero-gap energy bands and continuously tune the carrier density from holes to electrons via the Dirac neutrality point. Recent studies also addressed the spin degree of freedom, resulting in successful injection, transport and detection of spins in single and multiple layers of graphene [3–8]. The spin relaxation time τ_{sf} measured about 150 ps (as extracted from Hanle type spin precession measurements), which combined with a diffusion constant of $D \simeq 0.02$ m^2/s yielded a considerable room temperature spin diffusion length $\lambda_{sf} = \sqrt{D\tau_{sf}}$ of 1.5 to 2 μm.

8.2 Experiment

Until now, spin transport in graphene was studied in the low bias regime where the transport is described by diffusion only. In this paper we study the spin transport in the presence of DC electric fields. Due to the large carrier mobilities in graphene [9], the DC fields give rise to spin drift effects which are comparable in magnitude to the spin diffusion in graphene and, therefore, become accessible experimentally. In order to study the spin drift effect, we have built lateral spin valve devices as illustrated in Fig. 8.1. The graphene layer is contacted by a series of Co electrodes (F1-F5) used for the injection/detection of spins and the application of the DC electric fields. The dimensions of the contacts and their spacings given in the figure caption are the ones of the sample discussed in this paper and are characteristic for the spin valves we have fabricated. The graphene flakes we use are typically between 0.2 and 4 μm wide and up to 50 μm long. Besides the AFM thickness characterization of every flake, on several samples we have conducted Raman spectroscopy measurements as well [10], in order to select the single layer flakes. For a detailed description of the device fabrication see Ref. [3]. The contact resistances are between 2.5 kΩ and 12 kΩ. A standard low-frequency AC lock-in technique with a current of 4 μA RMS was used for measuring the spin signals. The measurements were performed at room temperature and in vacuum in order to minimize the shifts of the Dirac point due to charging effects of adsorbates on the graphene layer.

An AC spin imbalance is created in graphene by injection/extraction of spin currents by the ferromagnetic electrodes F4 and F5 through an aluminium-oxide tunnel barrier. Due to the opaque Co/Al_2O_3/graphene interface, the spin transport is not disturbed by the central contact F3. The spin imbalance diffuses

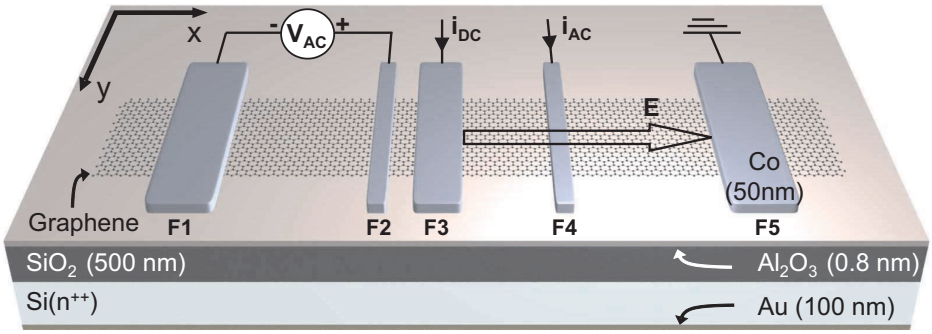

Figure 8.1: Schematic drawing of the spin drift experiment. The Co contact widths are 350 nm (for F1), 90 nm (F2), 250 nm (F3), 90 nm (F4), 350 nm (F5) and the distances between them are (from left to right) 2 μm, 0.6 μm, 1.3 μm and 2 μm. The 0.9×7 μm^2 sized graphene flake is covered by an aluminum oxide layer. A (gate) voltage, applied between the Au contacted Si(n^{++}) substrate and the grounded electrode F5, allows for the control of the charge density in graphene. The layer thicknesses are given in the brackets.

symmetrically, with respect to the injection points F4 and F5, through the device giving rise to an AC voltage drop between the ferromagnetic detector electrodes F2 and F1. In this non-local measurement geometry, the spin transport is thus completely separated from the charge transport and is solely described by the diffusion constant D and the spin relaxation time τ_{sf}. The non-local voltage drop between F2 and F1 is measured as a function of a magnetic field applied along the easy axis of the Co electrodes (y direction). This results in typical spin valve signals as shown in Fig. 8.2 a). The variable width of the Co electrodes yields a difference in their coercive fields (20 to 50 mT in the present case), allowing for separate switching in the external magnetic field. Contacts with similar widths, however, can sometimes interchange in their switching order depending on, e.g., the domain wall nucleation, on the sweeping direction of the field (positive to negative values and vice versa). Such an effect is observed in the measurement shown in Fig. 8.2 a) where the switching order of F4 and F5 is interchanged on the negative versus positive field's side. The identification of the switches could nevertheless be done by examining the spin valve signals obtained in different regions of the same sample by choosing different pairs of injector/detector electrodes.le by choosing different pairs of injector/detector electrodes.

Each discrete resistance level seen in Fig. 8.2 a) corresponds to a combination of magnetically parallel/antiparallel electrodes. The step heights carry information about the importance of that specific electrode's contribution to the spin injection/detection process. The highest change in signal is observed when the

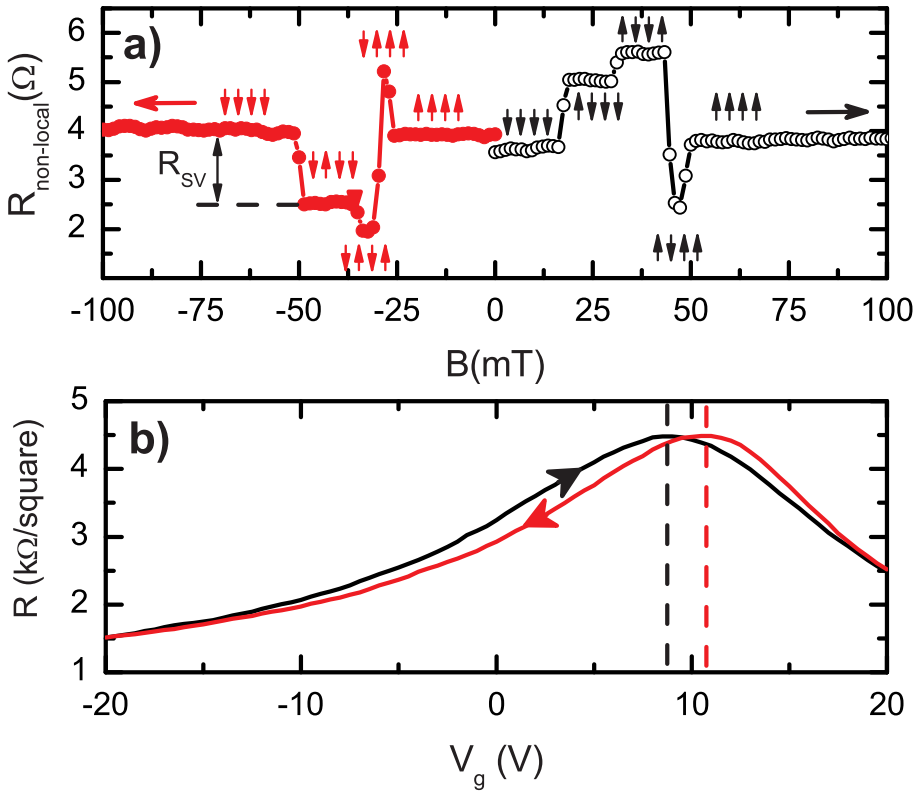

Figure 8.2: a) Non-local spin valve measurement of the device presented in Fig. 8.1. The small arrows represent the magnetic orientation of electrodes F1, F2, F4 and F5. The asymmetric spin valve behavior is due to the switching order of F4 and F5 which depends on external field sweep direction (indicated by the large horizontal arrows). R_{SV} represents the spin signal; see text for details. b) 4-point measurement of the graphene resistivity between contacts F3 and F4 versus the gate voltage.

inner electrodes (F2,F4) change their relative parallel/antiparallel magnetization state. The further away an electrode is, the smaller its corresponding resistance step is. The spins injected at F5 must diffuse longer (and have thus higher chance to relax) before they are detected by the detectors (F2,F1) than the spins injected at F4. The presence of four switches in our measurements proves the spin transport through the graphene channel under all magnetic electrodes, over the full $\simeq 6$ μm length of the device.

Spin drift effects in all-electrical n-GaAs based devices were measured by Lou *et al.* [11], where the conduction was limited to electrons. Unlike in semicon-

ductors, in graphene, due to its band structure, electrostatic gating allows for switching from hole to electron conduction while keeping the carrier mobility, diffusion constant, Fermi velocity, electric conductivity and other parameters approximately unchanged. The gating effect is reflected in the graphene resistivity as plotted in Fig. 8.2b). The position of the Dirac neutrality point separating hole and electron conduction regimes, as identified by the minimum in conductance [12, 13], shows a small hysteresis (+ 9 V to + 11 V) for the two sweep directions. The measurement also reveals a carrier mobility of μ =0.25 m^2/Vs.

Applying a DC electric field to generate carrier and spin drift in addition to the diffusion would in principle be possible by passing a DC current from F2 to F4. However, a strong DC bias can dramatically influence the spin injection efficiency of the electrodes [14,15] making it impossible to separate the drift effect contribution. We have conducted experiments on graphene spin valve devices where both AC spin injector electrodes are DC biased and we measured changes of the spin valve effect up to an order of magnitude compared to the non-biased measurements [16]. In order to avoid the manipulation of the spin injection efficiency, we have introduced the electrode F3 (see Fig.8.1). The DC field is applied between the electrodes F3 and F5 by sending a constant DC current between them, with F5 being grounded. We could not avoid sharing the drain of the AC and DC circuits, the injector F5 on the far right of the device is effectively DC biased. However, the effect of changing its injection efficiency with the DC current bias is minimized as discussed later.

Experimentally, the drift will manifest itself as an asymmetric distribution of the spin imbalance on the two sides of the spin injection point F4 (and F5), in addition to the symmetric diffusion process. Between F3 and F5 thus, where the field E is active, a favored direction of the spin transport will be defined by the electric field's polarity and the carrier type (electrons or holes). Such a device with fixed-distance injector/detector electrodes will therefore show a variable spin signal dependent on the DC electric field.

In Fig. 8.3 we present room temperature spin valve measurements for several DC currents (applied between F3 and F5) at three gate voltages: -20 V (hole conduction), +9 V (the Dirac neutrality point) and +38 V (electron conduction). The upper limit of the electric fields was set by the current densities allowed to pass through the tunnel barriers without damaging them[2]. Before each measurement, the magnetic field is ramped up to 300 mT to saturate the magnetization of the contact electrodes. The DC currents used were $\pm$40, $\pm$20 and 0 μA and their corresponding electric fields were $\pm$68 kV/m, $\pm$34 kV/m for V_g=-20 and +38 V and $\pm$206 kV/m, $\pm$103 kV/m for V_g=+9 V. Similar measurements, done on a set

[2]We have sent DC currents as high as 80 μA through a similar device, at which point the Co/Al_2O_3 electrodes were damaged.

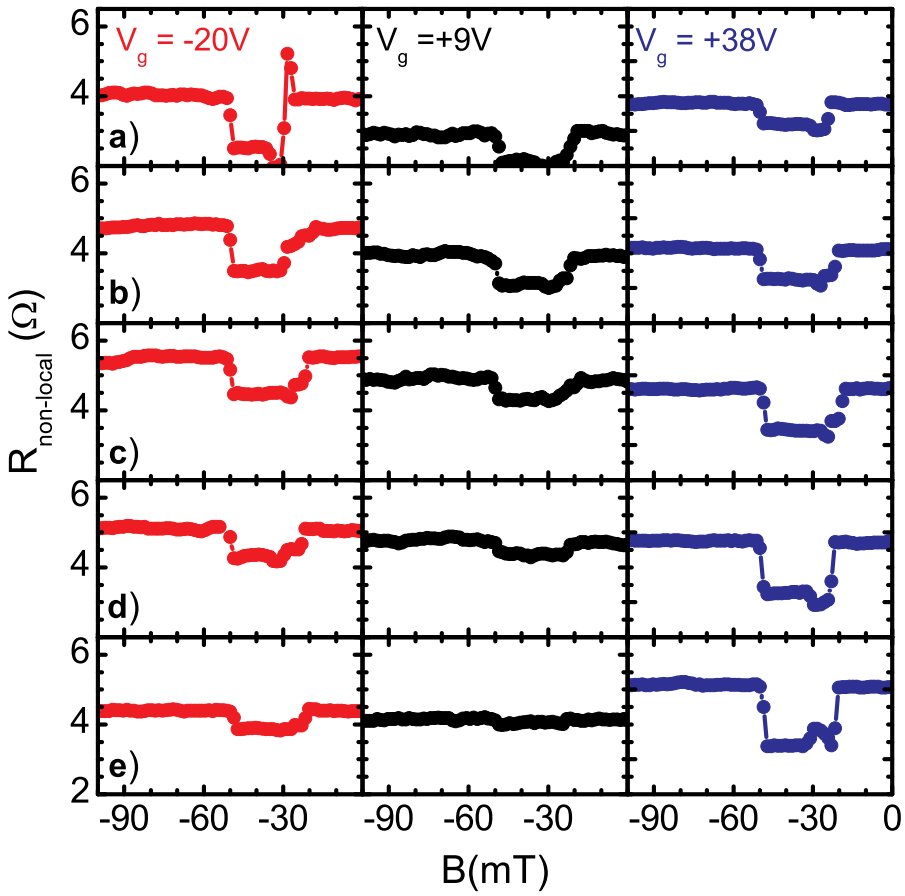

Figure 8.3: The drift effect in a graphene spin valve. The gate voltage V_g varies from left to right and it is indicated for each column. The DC electric current varies from top to down as: (a) I_{DC} = -40 μA, (b) -20 μA, (c) 0 μA, (d)+20 μA, (e) +40 μA. For clarity only the negative side of the spin valve measurements are plotted.

of samples with different geometry and/or contact resistances, support the data we present and discuss here.

The change in the injection efficiency of the electrode F5 (common ground for the DC and AC currents) for different DC fields appears in the spin valve measurements as an increased/decreased contribution of this electrode to the device non-local resistance. This can be seen in Fig. 8.3 where, for the measurements performed at +38 V gate voltage, the resistance step at approximately -30 mT

(corresponding to the magnetic switch of electrode F5) does show a dependence on the DC electric field. However, this electrode is positioned far from the AC detection circuit, and we can minimize its effect by defining the "spin signal" R_{SV} as the resistance step between the parallel and antiparallel magnetic state of the two *central* electrodes F2 and F4 (see Fig. 8.2). Therefore, the DC field dependence of R_{SV} indicates the presence of carrier drift as explained below.

At -20 V gate voltage (left column of graphs in Fig. 8.3), we are in the high density hole conduction regime with a carrier concentration of $n_h \simeq 3.5\times10^{16}$ m^{-2} yielding a graphene resistivity $R_{square} \simeq 1.5$ kΩ. The non-local spin signal R_{SV} reads 1 Ω when no DC field is present (graph c). Applying a DC field of +34 kV/m (graph d) and +68 kV/m (graph e) decreases the spin valve signal to 0.7 Ω and 0.45 Ω respectively, indicating spin drift in the region F3-F5 that counteracts the symmetric spin diffusion. This transport is labeled as "upstream" since, in order to detect a spin valve signal at electrodes F2 and F1, the spins need to travel against the action of the carrier drift. Now, if the DC electric fields' polarity is reversed, i.e. we apply a field of -34 kV/m (graph b) and -68 kV/m (graph a), the resulting drift facilitates spin transport towards the detectors ("downstream" transport) and the measured spin valve signal increases to 1.3 and 1.5 Ω respectively.

In the case of electron conduction, the drift effect reverses, because the electric field - charge carrier interaction is opposite, as seen in the set of curves measured at V_g=+38 V (right column in Fig .8.3). This voltage was selected to give approximately the same parameters (n_e, R_{local}) on the electron conduction side of the Dirac neutrality point as for the hole conduction (V_g=-20 V). The spin signal scales with the field amplitude and direction as expected, reading 0.6, 0.9, 1.2, 1.5 and 1.7 Ω for -68, -34, 0, +34 and +68 kV/m respectively.

At a gate voltage that locates the Fermi level close to the Dirac neutrality point ($R_{square} \simeq 4.5$ kΩ) the conduction happens neither via electrons, nor via holes, which means that no spin drift should take place. Examining the measurements at V_g=+9 V (central column of graphs in Fig. 8.3), we observe a slight decreasing tendency of the spin valve signal for increasingly positive DC fields, similar to the drift in case of hole conduction. This behavior can be explained by the interplay of the following two effects.

First, under the high DC current a certain shift of the effective gate voltage is expected. Considering the 20 kΩ resistance of the structure (graphene + contact F5), this shift equals to ±0.8 V for currents of ±40 μA. Unlike in the case of high carrier densities, around the neutrality point such a shift can critically change the carrier density in graphene and lead to spin drift. Second, due to a shift of the Dirac point in time under a constant gate voltage stress, it is difficult to set and keep a gate voltage just at the right position to assure neutrality. In our case,

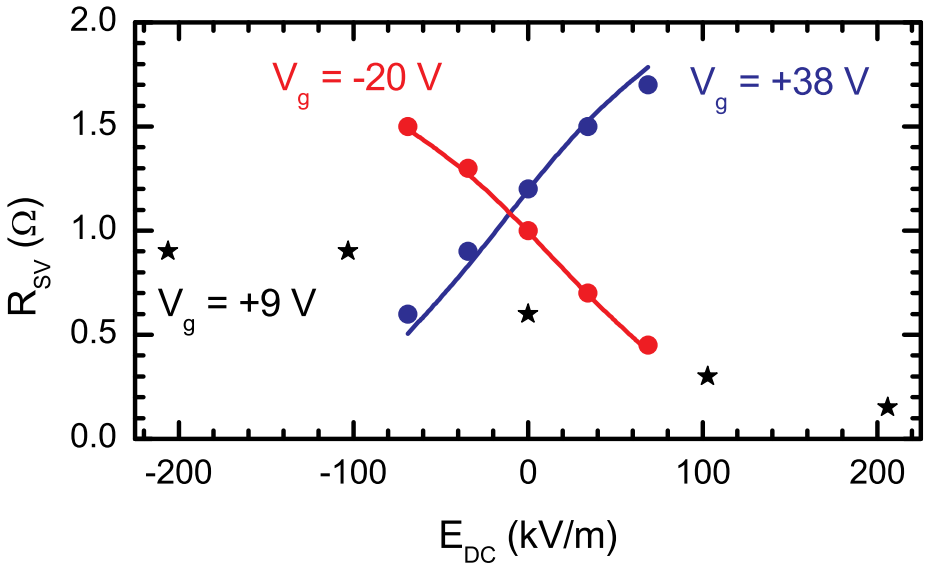

Figure 8.4: Spin valve signal for high carrier densities (circles), and near the Dirac neutrality point (stars). The lines represent a calculation (with no free parameters) of the drift effect based on the drift-diffusion equation.

it seems that we were slightly in the hole conduction regime when measuring at V_g=+9 V.

For a quantitative interpretation of the data we have extracted the spin signal values from all the measurements of Fig. 8.3 and plotted them in Fig. 8.4 against the DC field for the three gate voltages. For the theoretical description, we adopt the drift-diffusion model introduced by Yu and Flatté [14,17]. In the steady-state, the drift-diffusion equation for the spin imbalance n_s reads:

$$D\nabla^2 n_s + \mu E \nabla n_s - \frac{n_s}{\tau_{sf}} = 0, \tag{8.1}$$

where D is the diffusion constant, τ_{sf} is the spin relaxation time, μ is the carrier mobility and E is the DC electric field. The term μE represents the drift velocity v_d and its magnitude compared to the Fermi velocity $v_F = 10^6$ m/s is important for the contribution of the spin drift to the spin transport. Similar to the spin diffusion length $\lambda_{sf} = \sqrt{D\tau_{sf}}$, we define a spin drift length $\lambda_d = D/v_d$. The symmetric diffusion and asymmetric drift effects add up to form a spin transport characterized by a pair of length scales, named *upstream* and *downstream* lengths

$\lambda_\pm$ [17]:

$$\frac{1}{\lambda_\pm} = \pm\frac{1}{2}\frac{1}{\lambda_d} + \sqrt{\frac{1}{4}\frac{1}{\lambda_d^2} + \frac{1}{\lambda_{sf}^2}}. \tag{8.2}$$

The general solution to the spin imbalance equation 8.1 in the direction x parallel to the spin transport is

$$n_s(x) = A\exp(+\frac{x}{\lambda_+}) + B\exp(-\frac{x}{\lambda_-}), \tag{8.3}$$

where A and B are determined by the boundary conditions. Since we take the electrode F4 as the spin source, only the decaying solution with respect to the injection point need to be considered. Therefore, we can write the spin signal (R_{SV}) dependence versus the applied DC field in the form:

$$R_{SV} = R_0\exp(-\frac{L}{\lambda_\pm}), \tag{8.4}$$

where R_0 is the spin signal that would be measured at the injection point, $\lambda_\pm$ carries the electric field dependence (Eq. 8.2) and $L \simeq 1.5\mu$m is the distance between F3 and F4.

In the following we compare the drift-diffusion equation for the spin signal (Eq. 8.4) with the spin drift measurements in the high carrier density regime. From the conductivity measurements presented in Fig. 2b we extract $\mu \simeq 0.25$ m^2/Vs using $\sigma = ne\mu$, where the carrier concentration n is calculated from the sample's response to gate voltage (fig. 2b), using the method described in Refs. [2,13]. This gives a drift velocity of $v_d \simeq \pm 1.7\cdot 10^4$ m/s for $E \simeq \pm 68$ kV/m. The diffusion constant of $D \simeq 0.02$ m^2/s is obtained using the Einstein relation $\sigma = Ne^2D$, where the density of states N is determined according to Ref. [3]. Using Eq. 8.2 and a spin relaxation length $\lambda_{sf} \simeq 2\mu$m [3], we calculate the magnitude of the drift effect manifesting in the up/downstream lengths as $\lambda_+ = 1.3\mu$m, $\lambda_- = 3.0\mu$m for E $=\pm 34$ kV/m and $\lambda_+ = 0.9\mu$m, $\lambda_- = 4.4\mu$m for E $=\pm 68$ kV/m. Note, that at E $=\pm 68$ kV/m the characteristic length scale of the drift-diffusion spin transport is about two times increased/decreased compared to the diffusion process. The value of R_0 we estimate from the spin valve measurements in zero electric field when $\lambda_\pm = \lambda_{sf}$ and R_0 is given by $R_0 = R_{SV}\exp(L/\lambda_{sf})$. By taking the length of the drift region $L = 1.5\mu m$, $\lambda_{sf} = 2\mu m$ and the measured R_{SV} at E $=0$ we can determine R_0. Now, we are able to calculate the drift effect according to Eq. 4, all parameters being known. The theoretical curves (solid lines in Fig. 8.4) are in excellent agreement with the experimental data. There are no free parameters in the calculation and, in fact, these measurements could be used to extract λ_{sf}, if it would be unknown.

At the Dirac point, due to the symmetry, no drift effect is expected. However, in our measurements we are probably slightly away from the Dirac point. Here

we cannot apply our above analysis. It remains an open theoretical question to what the drift velocity should be at the charge neutrality point.

8.3 Conclusions

In conclusion, we studied spin transport manipulation in graphene, by carrier drift under the action of a DC electric field. For high charge carrier densities ($n \simeq 3.5 \times 10^{16}$ m^{-2}) depending on the direction of the applied DC field and the nature of the carriers we were able to modify the effective spin relaxation length by factor of 4.8 which resulted in a modulation of the spin valve signal of about 300%. The spin-drift measurements are described well by a drift-diffusion model. The control over the drift velocity we demonstrated opens new possibilities for exploring spin related phenomena in other types of graphene devices, such as graphene p-n junctions.

References

[1] K. S. Novoselov, *et al.*, *Science* **306**, 666 (2004)

[2] A. K. Geim, K. S. Novoselov, *Nature Materials* **6**, 183-191 (2007)

[3] N. Tombros, *et al.*, *Nature* **448**, 571 (2007).

[4] E. W. Hill, *et al.*, *IEEE Trans. Magn.* **42 (10)**, 2694 (2006)

[5] S. Cho, Y. F. Chen, M. S. Fuhrer, *Appl. Phys. Lett.* **91**, 123105 (2007)

[6] M. Nishioka, A. M. Goldman, *Appl. Phys. Lett.* **90**, 252505 (2007)

[7] M. Ohishi, *et al.*, *Jpn. J. Appl. Phys.* **46**, No. 25, L605-L607 (2007)

[8] W. H. Wang, *et al.*, *Phys. Rev. B* **77**, 020402(R) (2008)

[9] K. I. Bolotin, *et al.*, arXiv:0802.2389 (2008)

[10] A. C. Ferrari, *et al.*, *Phys. Rev. Lett.* 97, 187401 (2006)

[11] X. Lou, *et al.*, *Phys. Rev. Lett.* **96**, 176603 (2006) and references therein.

[12] K. S. Novoselov, *et al.*, *Nature* **438**, 197 (2005).

[13] Y.-W. Tan, *et al.*, *Phys. Rev. Lett.* **99**, 246803 (2007)

[14] Z. G. Yu, M. E. Flatte, *Phys. Rev. B* **66**, 235302 (2002)

[15] X. Lou, C. Adelmann, *et al.*, *Nature Physics* **3**, 197 (2007)

[16] C. Jozsa, *et al.*, in preparation

[17] Z. G. Yu, M. E. Flatte, *Phys. Rev. B* **66**, 201202(R) (2002)